

2012

A Two Photon Absorption Laser Induced Fluorescence Diagnostic For Fusion Plasmas

R. M. Magee

M. E. Galante

D. McCarren

E. E. Scime

R. L. Boivin

See next page for additional authors

Follow this and additional works at: https://researchrepository.wvu.edu/faculty_publications

Digital Commons Citation

Magee, R. M.; Galante, M. E.; McCarren, D.; Scime, E. E.; Boivin, R. L.; Brooks, N. H.; Groebner, R. J.; Hill, D. N.; and Porter, G. D., "A Two Photon Absorption Laser Induced Fluorescence Diagnostic For Fusion Plasmas" (2012). *Faculty Scholarship*. 453.
https://researchrepository.wvu.edu/faculty_publications/453

This Article is brought to you for free and open access by The Research Repository @ WVU. It has been accepted for inclusion in Faculty Scholarship by an authorized administrator of The Research Repository @ WVU. For more information, please contact ian.harmon@mail.wvu.edu.

Authors

R. M. Magee, M. E. Galante, D. McCarren, E. E. Scime, R. L. Boivin, N. H. Brooks, R. J. Groebner, D. N. Hill,
and G. D. Porter

A two photon absorption laser induced fluorescence diagnostic for fusion plasmas^{a)}

R. M. Magee,^{1,b)} M. E. Galante,¹ D. McCarren,¹ E. E. Scime,¹ R. L. Boivin,² N. H. Brooks,² R. J. Groebner,² D. N. Hill,² and G. D. Porter³

¹Physics Department, West Virginia University, Morgantown, West Virginia 26506, USA

²General Atomics, San Diego, California 92121, USA

³Lawrence Livermore National Laboratory, Livermore, California 94550, USA

(Presented 9 May 2012; received 7 May 2012; accepted 21 May 2012; published online 5 June 2012)

The quality of plasma produced in a magnetic confinement fusion device is influenced to a large extent by the neutral gas surrounding the plasma. The plasma is fueled by the ionization of neutrals, and charge exchange interactions between edge neutrals and plasma ions are a sink of energy and momentum. Here we describe a diagnostic capable of measuring the spatial distribution of neutral gas in a magnetically confined fusion plasma. A high intensity (5 MW/cm^2), narrow bandwidth (0.1 cm^{-1}) laser is injected into a hydrogen plasma to excite the Lyman β transition via the simultaneous absorption of two 205 nm photons. The absorption rate, determined by measurement of subsequent Balmer α emission, is proportional to the number of particles with a given velocity. Calibration is performed *in situ* by filling the chamber to a known pressure of neutral krypton and exciting a transition close in wavelength to that used in hydrogen. We present details of the calibration procedure, including a technique for identifying saturation broadening, measurements of the neutral density profile in a hydrogen helicon plasma, and discuss the application of the diagnostic to plasmas in the DIII-D tokamak. © 2012 American Institute of Physics. [<http://dx.doi.org/10.1063/1.4728092>]

I. INTRODUCTION: THE EVOLUTION OF TALIF

Active spectroscopy with laser induced fluorescence (LIF) is a valuable plasma diagnostic technique, providing localized measurements of neutral and ion velocity distributions. Since it was first demonstrated 35 years ago,¹ it has evolved into a workhorse plasma diagnostic. It has been used to diagnose ion temperature anisotropy in a helicon plasma,² measure turbulence in a magnetic nozzle,³ and measure neutral densities in the edge of a hot fusion plasma.⁴ Its development has been driven largely by the development of laser technology. In fact, since reliable, high energy, narrow spectral width lasers have become commercially available, a major step in LIF evolution has been reached: the progression to two photon absorption laser induced fluorescence, or TALIF.

TALIF has several advantages over traditional LIF. First, because two photons are used for excitation, each needs only provide half of the transition energy. This allows the direct excitation of the ground state with near-UV ($\lambda = 205 \text{ nm}$) photons, which are less expensive to produce and easier to transmit than $\lambda = 102.5 \text{ nm}$ photons. Second, the signal is proportional to the square of the laser intensity, rather than the intensity, so the measurement can be made highly localized without a perpendicular viewing chord. By focusing the injected beam with a lens, the TALIF signal is increased 10^5 times at the focus relative to the unfocused beam. For comparison, the LIF signal would only be 300 times larger at the focus. (This is for the case used here: lens focal length

$f = 25 \text{ cm}$, beam divergence $\theta = 0.5 \text{ mrad}$, and initial beam radius $r = 0.2 \text{ cm}$). Finally, the TALIF diagnostic has the ability to make a Doppler-free measurement by employing two counter-propagating beams, where the energy of a photon from each beam sums to the transition energy for all atom velocities. Practically, this means that the time resolution of density measurements is increased as there is no need to scan the laser frequency.

Here we employ the three level hydrogen scheme first demonstrated by Bokor *et al.*⁵ Ground state hydrogen is excited from the $n = 1$ level to the $n = 3$ level by the simultaneous absorption of two $\lambda \sim 205 \text{ nm}$ photons. After excitation, a fraction of the hydrogen atoms decay from the $n = 3$ level to the $n = 2$ level and emit photons at 656.3 nm which are collected. Note that TALIF is *absorption* spectroscopy, so the measured signal is related to the Doppler-shift of the absorbed light, rather than the emitted light.

The West Virginia University TALIF system builds on previous work^{6,7} by combining for the first time both high power and narrow spectral width. This results in larger signal levels, an important feature for measurements in fusion plasma where the background emission is high. It also means that the line is more easily saturated, which leads to artificial broadening.

II. LASER AND LIGHT COLLECTION HARDWARE

A dye laser is pumped by a Spectra-Physics Quanta-Ray Pro-270 pulsed Nd:YAG laser with a maximum power of 600 mJ per pulse at 532 nm at a repetition rate of 20 Hz. The pulses have been measured to be 10 ns wide (i.e., $P_{inst} \sim 100 \text{ MW}$) with 2% energy stability.

^{a)}Contributed paper, published as part of the Proceedings of the 19th Topical Conference on High-Temperature Plasma Diagnostics, Monterey, California, May 2012.

^{b)}Email: richard.magee@mail.wvu.edu.

The dye laser is a Sirah CobraStretch optimized for 615 nm light with a mixture of Rhodamine B and Rhodamine 101. The grating (2400 l/mm) yields a measured linewidth of 0.07 cm^{-1} . The energy is $\sim 150 \text{ mJ/pulse}$ and the pulse width is 12 ns (i.e., $P_{inst} \sim 10 \text{ MW}$).

The output of the dye laser is frequency doubled to 308 nm in a SHG-250 BBO crystal, mixed back with the 615 nm fundamental, and passed through a SHG-206 BBO crystal to generate a third harmonic beam at 205 nm. The 205 nm light has a maximum power of 8.5 mJ/pulse, a temporal FWHM of 7 ns (i.e., $P_{inst} \sim 1 \text{ MW}$), energy stability of 5%-7% and a spatial profile very nearly Gaussian with a width of $\sigma = 1.7 \text{ mm}$. The linewidth of the 205 nm beam can be calculated from the measured 615 nm beam: $\Delta k_{205} = \sqrt{3}\Delta k_{615} = 0.12 \text{ cm}^{-1}$.

The collected light is filtered with a $656.3 \pm 0.5 \text{ nm}$ band-pass filter and focused onto a photomultiplier tube (PMT) (Hamamatsu H11526-20-NF). The PMT output is amplified with a high speed amplifier (Hamamatsu C5594) that has an operating range of 50 kHz–1.5 GHz and a gain of 36 dB. The amplified PMT signal is then processed by a Stanford Research Systems Fast Gated Integrator and Boxcar Averter (Model SR250). The boxcar acquires data at twice the repetition rate of the laser, so that signal and background measurements are interleaved. The background is subtracted from the laser pulses, and they are integrated in time and averaged together. The result is recorded along with the measured wavelength of the 615 nm beam, obtained with a High Finesse WS7 wavelength meter that is accurate to 0.075 pm or 60 MHz. The laser is scanned in wavelength across the distribution in 1s or 10s of seconds. Typically, as shown in the inset of Figure 2, 400 data points are collected and smoothed by 10.

III. TALIF CALIBRATION AND MEASUREMENTS

The TALIF signal amplitude as a function of laser frequency, omitting constants, is

$$S(\nu) \sim \frac{I^2 n_0}{\sqrt{\Delta \nu_d^2 + 2\Delta \nu_l^2}}. \quad (1)$$

It is proportional to the square of the laser intensity, I , and the neutral density, n_0 . The Doppler and laser linewidths, $\Delta \nu_d$ and $\Delta \nu_l$, respectively, appear in the denominator, indicating that the signal amplitude drops with increased temperature or decreased laser performance.

The line shape of the TALIF signal is a convolution of the particle velocity distribution and the distribution of photon pairs (which is twice the laser linewidth). In the case where both of these are Gaussian, the width of the signal is given by,

$$\Delta \nu_s = \frac{1}{2} \sqrt{2\Delta \nu_l^2 + \Delta \nu_d^2}.$$

Absolute calibration of the diagnostic is accomplished by generating a TALIF signal from a known pressure of krypton gas.^{6,9,10} The excitation wavelength for the $4p^6 1S_0$ to $5p^6 [3/2]_2$ transition in ground state krypton is at 102.1 nm (i.e., $2 \times 204.2 \text{ nm}$ photons) and the emission from the $5p^6 [3/2]_2$ to $5s^6 [1/2]_1$ transition is at 826 nm, making it an ideal calibration scheme.¹⁰ The absolute atomic hydrogen

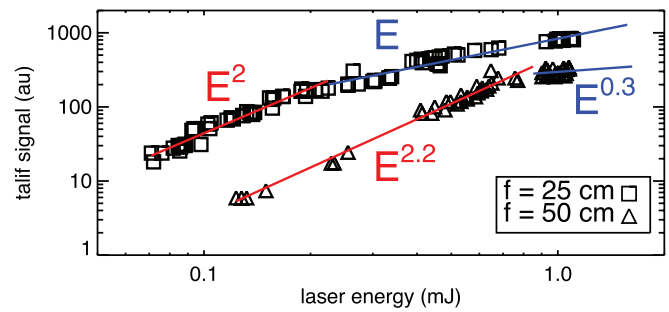


FIG. 1. Measured TALIF signal from KrI (symbols) scales very nearly as E^2 (red curves) until the critical saturation intensity is reached. This occurs for $E = 0.22 \text{ mJ}$ with an $f = 25 \text{ cm}$ lens (squares) and $E = 0.85 \text{ mJ}$ for an $f = 50 \text{ cm}$ lens (triangles). The critical energy is four times larger in the latter case because the spot size is twice as large.

density in plasma is determined from the ratio of the TALIF signals when the relative detection sensitivities for the two species is known.

When the number of particles to be pumped in a laser pulse time exceeds the number of particles available in the emission volume, the line is saturated. Because this happens first in the wings of the distribution, where there are fewer particles, exceeding the critical laser intensity broadens the line, a process referred to as saturation broadening.⁸ If the laser pulse length is shorter than the relaxation time of the transition, the critical intensity can be approximated as, $I_c \approx \frac{\hbar\omega}{\beta\sigma_{2\gamma}g\tau}$, where \hbar is Planck's constant, ω is the laser frequency, β is a statistical photon counting factor, $\sigma_{2\gamma}$ is the two photon absorption cross section, g is the absorption line shape, and τ is the laser pulse time. For the case of cold Kr, we expect the laser to saturate the line at $I_c = 3 \times 10^8 \text{ W/cm}^2$.

Shown in Figure 1 are the amplitudes of the Kr TALIF signal as a function for laser energy for two cases: one with an $f = 25 \text{ cm}$ injection lens and one with an $f = 50 \text{ cm}$ injection lens. In the $f = 25 \text{ cm}$ case, the functional dependence of the amplitude changes from E^2 to E at $E = 0.22 \text{ mJ}$ (corresponding to an intensity of $2 \times 10^8 \text{ W/cm}^2$ assuming a focused beam size of $r = 70 \mu\text{m}$). When the focal length of the injection lens is doubled, the radius of the focused beam spot is doubled, and the critical laser energy increases to $E = 0.85 \text{ mJ}$, very nearly a factor of four. As the energy is increased beyond the critical energy the line is broadened. If this effect is not avoided or accounted for, one could interpret sat-

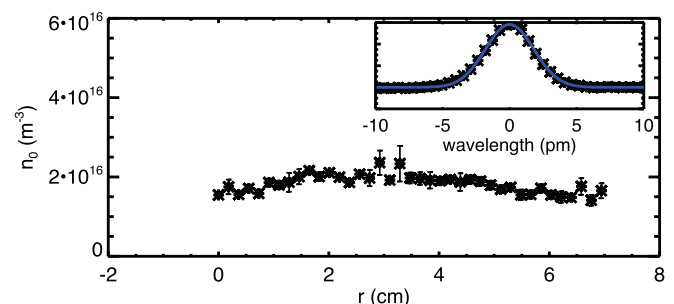


FIG. 2. Neutral density radial profile across the plasma expansion chamber with example spectrum inset.

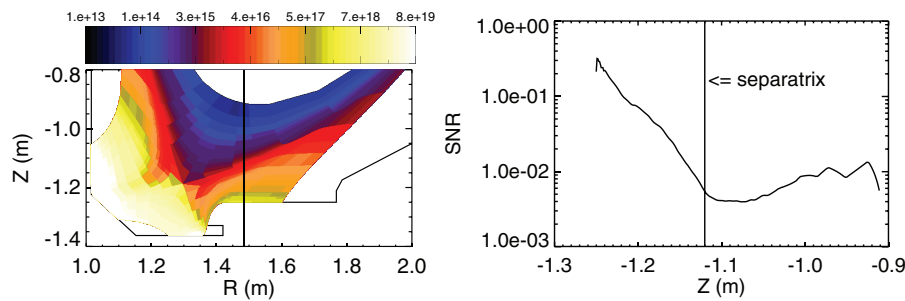


FIG. 3. The neutral density predicted for DIII-D by the UEDGE code in m^{-3} (left), and the expected signal-to-noise ratio (right). With averaging, SNR as low as 1% have been resolved in the test plasma, implying that the neutral density can be measured up to the separatrix in DIII-D.

uration broadening as Doppler broadening, and overestimate both the temperature and density of the gas.

Hydrogen plasma is generated by an RF discharge (~ 600 W at ~ 13 MHz) in a glass tube with $D = 8$ cm and $L = 60$ cm and allowed to expand into a stainless steel chamber with $D = 14$ cm and $L = 25$ cm. There is an axial magnetic field of 10s-100s of G. Typical plasma parameters from Langmuir probe measurements are $n_e \approx 10^{10}$ – 10^{12} cm^{-3} and $T_e \approx 1$ – 10 eV.

The laser light is injected through a $D = 1$ cm hole drilled in a 45° turning mirror. The light is focused in the plasma, stimulating emission which is collected and collimated by the same lens, and turned by the mirror into a focusing lens mounted in front of a PMT. This “confocal” configuration allows the measurement of the neutral density profile by simply scanning the injection lens towards and away from the plasma source. The result of such a scan is shown in Figure 2. In these particular plasmas the neutral hydrogen density profile was found to be relatively flat.

IV. APPLICATIONS TO DIII-D PLASMAS

The neutral particles at the edge of a magnetically confined plasma represent both a particle source (plasma fueling via ionization) and a particle, energy, and momentum sink (energetic particle loss through charge exchange). The neutral density is therefore an important parameter in calculations of particle confinement time and plasma rotation. In tokamak plasmas, the neutral density profile is thought to play an important role in pedestal formation and the L- to H-mode transition. The neutral density is also important for interpretation of neutral particle energy analyzer data, where the velocity distribution of plasma ions is inferred from measured neutral velocities.

Neutral density measurements are challenging for two reasons. First, the background D_α levels tend to be high, due to significant amounts of electron impact excitation. Second, the neutral density can vary by several orders of magnitude over the desired measurement region. To quantify signal to background level, we investigate a specific case for the DIII-D tokamak.

The neutral density and D_α emission are modeled with UEDGE (unified edge code), a 2-D fluid code, which

solves the fluid equations for density, energy and parallel momentum.¹¹ Transport parallel to field lines is assumed to be classical while perpendicular transport is assumed to be anomalous with an artificial radial diffusion coefficient. The neutrals are treated as an inertial fluid that can interact (i.e., exchange momentum) with ions via charge exchange.¹² The output of a UEDGE run are T_e , n_e , and n_0 . An example of the neutral density is shown in Figure 3 for DIII-D discharge 142 613 at $t = 4500$ ms.

The outputs of the UEDGE code can be used to calculate the D_α emissivity, which has been benchmarked against the measured D_α emission to within a factor of 2. Because the TALIF measurement relies on a background subtraction to isolate the signal, the signal-to-noise ratio (SNR) depends on the size of the D_α fluctuations on the time scale of this subtraction ($t \sim 100$ ns). These data are not available, so we use the fluctuation amplitude on the $500 \mu\text{s}$ time scale, likely an upper bound. The result of the calculation is shown in Figure 3. We conclude that the signal is resolvable up to the separatrix in DIII-D.

ACKNOWLEDGMENTS

This work is funded by the US Department of Energy (DOE) through Grant No. DE-SC0004736.

- ¹R. A. Stern and J. A. Johnson, *Phys. Rev. Lett.* **34**, 1548–1551 (1975).
- ²E. E. Scime, P. A. Keiter, M. W. Zintl, M. M. Balkey, J. L. Kline, and M. E. Koepke, *Plasma Sources Sci. Technol.* **7**, 186–191 (1998).
- ³F. M. Levinton and F. Trintchouk, *Rev. Sci. Instrum.* **72**, 898–905 (2001).
- ⁴P. Mertens and M. Silz, *J. Nucl. Mater.* **241-243**, 842–847 (1997).
- ⁵J. Bokor, R. Freeman, J. White, and R. Storz, *Phys. Rev. A* **24**, 612–614 (1981).
- ⁶M. Boogaarts, S. Mazouffre, G. Brinkman, H. van der Heijden, P. Vankan, D. S. J. A. M. van der Mullen, and H. Döbele, *Rev. Sci. Instrum.* **73**, 73–86 (2002).
- ⁷T. Kajiwara, T. Shinkawa, K. Uchino, M. Masuda, K. Muraoka, T. Okada, M. Maeda, S. Sudo, and T. Obiki, *Rev. Sci. Instrum.* **62**, 2345–2349 (1991).
- ⁸W. Demtröder, *Laser Spectroscopy Volume 2: Experimental Techniques* (Springer, 2008).
- ⁹J. Jolly and J.-P. Booth, *J. Appl. Phys.* **97**, 103305 (2005).
- ¹⁰K. Niemi, V. Schulz-von der Gathen, and H. Döbele, *J. Phys D* **34**, 2330–2335 (2001).
- ¹¹T. D. Rognlien, J. L. Milovich, M. E. Rensink, and G. D. Porter, *J. Nucl. Mater.* **196-198**, 347–351 (1992).
- ¹²G. D. Porter, S. L. Allen, M. Brown, M. E. Fenstermacher, D. N. Hill, R. A. Jong, A. W. Leonard, D. Nilson, M. E. Rensink, T. D. Rognlien, G. R. Smith, and the DIII-D Team, *Phys. Plasmas* **3**, 1967–1975 (1996).